Simulation of Moisture-induced Shape Changes of Fused Layer Modeling (FLM) 3D Printed Wood/Polylactic Acid (PLA) Composites

Stefan Kain,[a,e,*] Josef V. Ecker,[b] Bettina Dorfner,[a] Andreas Haider,[c] Timothy M. Young,[d] Thomas Schnabel,[a] Maurizio Musso,[e] and Alexander Petutschnigg [a]

In recent years, the variety of materials for fused layer modeling (FLM) 3D printing has expanded considerably, and new smart materials such as shape memory polymers (SMPs) have been added. Such SMPs enable so-called 4D printing, a programmable shape transformation of FLM 3D printed objects over time due to an external stimulus such as moisture or temperature. This paper addresses the processing of a specially fabricated climate-responsive wood/polylactic acid (PLA) composite using FLM 3D printing and the application of varying print directions for manufacturing programmable shape changing objects. In addition, this study is about developing a two-dimensional mathematical model based on the linear difference method to forecast accurately the moisture-induced deformation behaviour of 4D printed objects. Furthermore, the occurring deformations of the 4D printed objects were recorded using 3D scanning technology and compared with the simulated deformations from the mathematical model for validation purposes. With the help of the developed two-dimensional mathematical model, an exact reproduction of the deformation behaviour of 4D printed objects was made with a deviation percentage of always less than 6.5%.

DOI: 10.15376/biores.21.2.3137-3157

Keywords: Shape memory polymers (SMPs); 4D Printing; Moisture-induced shape changing; Wood/PLA composite; Varying print directions; Mathematical model

Contact information: a: Department of Design and Green Engineering, Salzburg University of Applied Sciences, Markt 136a, 5431 Kuchl, Austria; b: Institute of Chemical Technologies and Analytics, Vienna Technical University, Getreidemarkt 9, 1060 Vienna, Austria; c: Department of Bio-based Composites and Processes, Wood K Plus – Kompetenzzentrum Holz GmbH, Altenberger Straße 69, 4040 Linz, Austria; d: Center for Renewable Carbon, University of Tennessee, Jacob Drive 2506, 37996-4570 Knoxville, Tennessee, USA; e: Department of Chemistry and Physics of Materials, University of Salzburg, Jakob-Haringer-Straße 2a, 5020 Salzburg, Austria;
** Corresponding author: stefan.kain@fh-salzburg.ac.at*

INTRODUCTION

A variety of different materials that positively affect people's daily life are nature-inspired. These materials are very well adapted to their specific requirements and equipped with very unique functions. Pine cones, as an example, respond to various environmental conditions (warm or cold and dry or wet) by automatically opening their shells to release their seeds or keeping them closed for protection against external influences. Researchers are currently attempting to copy this behaviour of nature-based materials (*e.g.*, temperature- and/or moisture-induced changes in shape of specific materials) as a means to produce smart materials such as shape memory polymers (SMPs). These SMPs can be

processed using fused layer modeling (FLM), which is a filament-based 3D printing methodology. By developing an accurate mathematical model, the moisture-induced shape changing behaviour of such SMPs can be simulated as a function of prevalent climate conditions. These simulation results can be utilized to define suitable print directions that cause certain deformations in the printed object, resulting in 4D printing.

FLM 3D Printing

In principle, additive manufacturing (AM) including FLM 3D printing is capable of manufacturing simple objects as well as complex-shaped parts without additional costly modifications. This aspect can have a positive impact on product costs, especially when complex-shaped parts need to be produced (Wimmer *et al.* 2015). Due to an adequate material availability, extrusion-based 3D printing including FLM is currently by far the most common technology (Wang *et al.* 2018). 3D printed objects, in whatever form, are built by continuously depositing a controlled amount of material, layer by layer, onto a build plate until the physical model is completed. However, a sufficient stability of the first layer is required before the next layer can be deposited; otherwise, defects can occur, which impair print quality (Kirchmajer *et al.* 2015; Lee *et al.* 2017b).

Furthermore, FLM 3D printing, as a revolutionary production methodology, utilizes filaments as a means to achieve very efficient manufacturing with very little waste production. In the last decade, great emphasis has been put on the development of FLM 3D printing materials, including the use of biodegradable, natural, or recycled materials such as wood fibres, cellulose, as well as lignin (Wimmer *et al.* 2015).

Shape Memory Polymers (SMPs)

When it comes to smart materials, there is a very ambitious but also very promising issue dealing with the integration of programmable actuator technology into the material's structure. Over a very long time span, nature has formed numerous materials that are capable of adapting their intrinsic shape as well as specific properties in response to environmental stimuli, *e.g.*, heat or humidity (Studart 2015; van Rees *et al.* 2017; Arslan *et al.* 2019). Inspired by these nature-based materials (biomimetic structures), various international research groups are working intensively on stimulus-response materials as well as self-shaping materials based on SMPs (Arslan *et al.* 2019).

Basically, SMPs are known for having shifting stiffnesses, being programmable in an easy way, to tolerate very huge deflections without suffering fatigue-induced damage and to need only very little actuation forces for adjusting their internal shape (Clifford *et al.* 2017). Furthermore, they are easy to process and they have a wide range of interesting properties when it comes to mechanical performance and are generally cheap in production (Ratna and Karger-Kocsis 2008). The microstructure of SMPs enables the polymers to have intrinsic sensing, controlling, and actuating capacities (Thompson *et al.* 1992; Wei *et al.* 1998), allowing the materials to be sensors, controllers, as well as actuators all in one. Besides, no additional energy source is needed, which enables an electronic or mechanical control (Addington and Schodek 2005; Juaristi *et al.* 2018; Vazquez *et al.* 2019).

SMPs can react accordingly in a pre-determined manner once they detect variations in environmental conditions (Gandhi and Thompson 1992; Wei *et al.* 1998; Yu *et al.* 2015). As soon as such an external stimulus, *e.g.* humidity for hydro-active composites or temperature in case of thermo-active composites (Vazquez *et al.* 2019), disappears, the deformation is reversed by returning to its initial geometry (Gandhi and Thompson 1992; Wei *et al.* 1998). However, the usage of SMPs for stimulus-driven shape changes could

help to diminish the complexity of a system by reducing the dependence on digital computation, external sensors and electronics (Clifford *et al.* 2017), as SMPs are sensors, controllers, and actuators at the same time

Natural Fibre Compounds (NFCs) – Wood Filaments

Since pricing of numerous commercial polymers have noticeably increased in the past years, adding filler materials (*e.g.* natural fibrous materials including wood fibres) to the polymer is a well-established method, which will noticeably cut costs. In some cases, the addition of a fibrous filler to the polymer can also help to improve the performance (thermal properties as well as mechanical properties) of the material (Kim and Pal 2010; Ayrilmis 2018).

Additionally, natural fibrous materials including wood fibres have some substantial advantages compared to inorganic fibrous materials. Basically, their lightweight structure leads to a lower density, relatively low costs (on volumetric basis), flexibility in processing, and easy availability. Besides, a high specific stiffness, the renewable nature, their high specific moduli, and safe disposal are just a few of these advantages (Dominkovics *et al.* 2007; Faruk *et al.* 2012; Kaboorani 2017; Ayrilmis 2018). However, NFCs have a considerable disadvantage in terms of interfacial bonding between the polymer matrix and the natural fibrous material. The poor bonding properties are related to the divergent chemical nature of the components – in general, plastics are hydrophobic, whereas natural fibres are hydrophilic (Mohanty *et al.* 2002). Nevertheless, to improve the poor bonding properties of NFCs, coupling agents, *e.g.* maleic anhydride, can be added during the compounding process (Keener *et al.* 2004; Huang *et al.* 2021).

In general, wood is hygroscopic, meaning that it is capable of absorbing moisture from the surrounding, resulting in swelling, as well as to release moisture to the environment, leading to shrinking (Kaboorani 2017; Ayrilmis 2018; Kariz *et al.* 2018). However, the swelling and shrinking behaviour is anisotropic, implying that the extent of swelling and shrinking is direction-dependent (Pang 2002).

When finely chopped wood fibres are embedded in a polymer matrix, the wood filler transfers its hygroscopic properties to the compound. This means that these NFCs are also able to swell and shrink when exposed to various climatic conditions (Dányádi *et al.* 2010; Kaboorani 2017; Ayrilmis 2018; Kariz *et al.* 2018).

The moisture content (MC) of FLM 3D printed objects using NFCs can be affected by changing specific environmental atmospheric conditions, such as relative humidity and temperature. Alternatively, a change in MC can be achieved by directly wetting, moistening the surface, or submerging the complete object (Correa *et al.* 2015). In recent years, various scientific articles have been published showing that wood-based materials can be utilized for stimulus-induced shape change systems (Correa *et al.* 2015; Reichert *et al.* 2015; Zuluaga and Menges 2015; Gladman *et al.* 2016; Le Duigou *et al.* 2016; Vailati *et al.* 2018; Vazquez *et al.* 2019). Reichert *et al.* (2015) introduced several nature-inspired building designs that use the hygroscopic properties of moisture sensitive materials for shape changing. Le Duigou *et al.* (2016) applied wood-based bio-composites to create objects that deform in a particular way when exposed to moisture. A bilayer configuration for shading devices, enabling an autonomous operation, was successfully developed by Vailati *et al*. (2018). In terms of the bilayer configuration, each layer had completely divergent swelling coefficients. Gladman *et al.* (2016) used 3D printing to process hydrogel composites with embedded cellulose fibrils that change their shape when in contact with

water. Correa *et al.* (2020) designed hygro-responsive composite polymer sheds (scales) made from polymers containing cellulose fibrils and processed using 3D printing.

4D Printing – 3D Printing using SMPs

In principle, FLM can be used to program SMPs while depositing the material layer upon layer on the build plate, additionally; it is not necessary to apply any post-programming (Hu *et al.* 2017). If the object is produced in that way, unrestricted access to the entire surface of the printed object can be ensured, which is a substantial advantage (van Manen *et al.* 2018). As soon as the manufactured object is deformed by an external stimulus (*e.g.* humidity or temperature), access to the entire surface of the object is only possible to a limited extent.

Basically, the print direction during material deposition determines the orientation of the fibres embedded in the polymer matrix, which subsequently influences the behaviour of the shape change when exposed to a certain stimulus. In addition, there are some other parameters that influence the behaviour too, such as the layer height, the total number of printed layers, and a bilayer configuration. In terms of a bilayer configuration, the order in which active and constrained layers are deposited also has an influence on shape changing (Vazquez *et al.* 2019).

When FLM 3D printing is utilized for manufacturing three-dimensional objects, the material deposition can be managed (Correa *et al.* 2015) just by adapting the print direction (Kain *et al.* 2020). This makes it possible to carefully control the stimulus-induced shape change of FLM 3D printed objects very precisely, *i.e.* to control the curling process (Correa *et al.* 2015). Due to the aspect that 4D printing is a relatively novel approach for producing a stimulus-triggered change in shape, there are difficulties that need to be solved. One issue concerns the processability of SMPs, especially reversible SMPs, using 3D printing technologies (Lee *et al.* 2017a). Another aspect concerns the simulation as well as the 4D modelling. Conventional modelling programs, *e.g.* CAD programs, used for AM have problems representing the material properties at the micro-scale level, especially the characteristics of smart materials (Zafar and Zhao 2020). Independently of this, work still needs to be done on developing a simulation software that is capable to predict three-dimensional shape changing behaviour as a function of time.

However, in order to avoid complexity caused by too many influencing factors in the development of such 4D simulation software, the object should initially be of a simple structure and the deformation should be modelled with fewer dimensions, *i.e.* it should be started with a two-dimensional instead of a three-dimensional mathematical model.

Nevertheless, 4D printing could be very interesting and useful, *e.g.* in the fields of packaging, automotive, construction and medicine (Lee *et al.* 2017a).

Objective

The aim of this study was to develop a two-dimensional mathematical model that accurately predicts the moisture-induced deformation behaviour of FLM 3D printed NFCs. Furthermore, this model could be utilized to simulate the influence of specific print direction combinations on the moisture-induced deformation behaviour.

EXPERIMENTAL

Wood Filament – NFC Compound

For the investigations on the moisture-induced shape changing behaviour of FLM 3D printed objects, a specially fabricated moisture-sensitive wood filament was used. The filament was a wood/PLA composite consisting of 75 wt.% PLA and 25 wt.% wood fibres. This NFC reacts to an increase or decrease of the MC level with swelling or shrinking. A detailed description of the NFC preparation can be found in the publication by Kain *et al.* (2020).

Software

The simulation of the moisture-induced deformation behaviour of the samples were conducted utilizing the MATLAB R2018a software packages.

Instruments

All instruments which were utilized in the study are listed below in Table 1:

Table 1. Instruments Used for Sample Manufacturing, Experiments, and Analysis

Device	Model	Manufacturer
FLM 3D printer	Ultimaker 2+	Ultimaker B.V. (Geldermalsen, the Netherlands)
Climatic chamber	KBF 240	BINDER (Tuttlingen, Germany)
Drying and heating oven	FD 115	BINDER (Tuttlingen, Germany)
Calliper	CD-15CPX	Mitutoyo (Kawasaki, Japan)
Precision scale	PRS 620-3	KERN (Balingen, Germany)
3D scanner	Artec Space Spider	Artec 3D (Luxembourg, Luxemburg)

Testing of Moisture-Induced Swelling and Shrinking

Ten FLM 3D printed and identically shaped cuboids (illustrated in Fig. 1) with a length and a width of 50 mm as well as a height of 3 mm were used for testing the moisture-induced swelling and shrinking. A commercially available and unmodified Ultimaker 2+ from Ultimaker B.V. (Geldermalsen, the Netherlands) equipped with a 0.6 mm nozzle was utilized for FLM 3D printing the test specimens using the custom-made wood/PLA composite. A wall thickness of 1.2 mm (2 perimeters) was set and a line-infill direction was chosen for the printing process. All layers within a test specimen had an identical orientation in terms of infill direction. Further chosen process parameters can be found in the paper Kain *et al.* (2020). Depending on the relative humidity and the temperature in the climatic chamber, the MC and the differential swelling and shrinking behaviour were determined. These material characteristics served as database for the mathematical model to predict the deformation behaviour of FLM 3D printed objects under specific climatic conditions.

Six equally distanced measuring areas per specimen were marked to determine the differential swelling and shrinking behaviour (β), whereby three measuring sections were

parallel to the print direction ($\beta_{\parallel}$) and the others were orthogonal to the print direction ($\beta_{\perp}$). Afterwards, the test specimens were conditioned to constant weight in a climatic chamber from BINDER (Tuttlingen, Germany) at a temperature of 23 °C and 65% relative humidity.

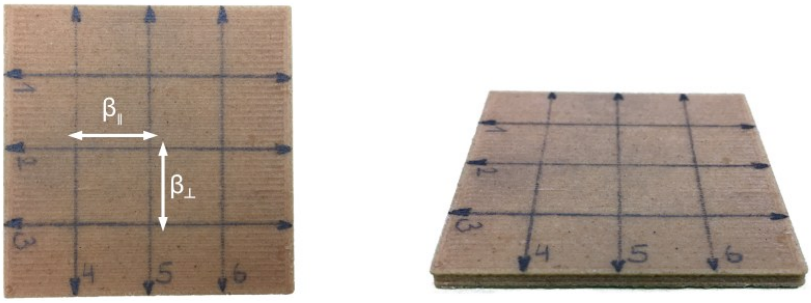

Fig. 1. One of 10 identically FLM 3D printed specimens for determining the differential swelling and shrinking behaviour as well as the MC. The marked measuring areas per test specimen are shown, three measuring sections being parallel to the print direction ($\beta_{\parallel}$) – No. 1, No. 2 and No. 3 – the other three being orthogonal to the print direction ($\beta_{\perp}$) – No. 4, No. 5 and No. 6

The samples were then exposed to a temperature of 23 °C and 85% relative humidity in the same climatic chamber. When constant weight was reached, the mass was weighed using a precision scale from KERN (Balingen, Germany). In addition, the moisture-induced swelling was determined by measuring the deviation of the six measuring sections per specimen, using a calliper from Mitutoyo (Kawasaki, Japan). This procedure was repeated for the climate with a temperature of 23 °C and 50% relative humidity as well as for a temperature of 23 °C and 35% relative humidity. Finally, the test specimens were dried in a dry kiln from BINDER at a temperature of 50°C until constant weight was reached. The final weight was measured, and the shrinkage of the specimens was determined.

Based on the measurements, Eqs. 1 and 2 were used to calculate the differential swelling and shrinking behaviour parallel ($\beta_{\parallel}$) and orthogonal ($\beta_{\perp}$) to the print direction. In general, the differential swelling and shrinking behaviour describes the relative dimensional change of a material in percent per 1% change in moisture content (MC) within the investigated relative humidity range between 35% and 85%.

The differential swelling and shrinking behaviour parallel to the print direction ($\beta_{\parallel}$) expressed as percent change per percent MC (%/%) was calculated as follows,

$$\beta_{\parallel} = \frac{l_{\parallel(85)} - l_{\parallel(35)}}{l_{\parallel(35)} \cdot (u_{(85)} - u_{(35)})} \cdot 100 \quad (1)$$

where $l_{\parallel(85)}$ and $l_{\parallel(35)}$ represent the specimen length [mm] measured at 85% relative humidity as well as 35% relative humidity and $u_{(85)}$ as well as $u_{(35)}$ denote the corresponding MC [%] of the specimens determined at 85% relative humidity and 35% relative humidity.

The differential swelling and shrinking behaviour orthogonal to the print direction ($\beta_{\perp}$) expressed as percent change per percent MC (%/%) was calculated analogously as follows,

$$\beta_{\perp} = \frac{l_{\perp(85)} - l_{\perp(35)}}{l_{\perp(35)} \cdot (u_{(85)} - u_{(35)})} \cdot 100 \quad (2)$$

where $l_{\perp(85)}$ and $l_{\perp(35)}$ represent the specimen length [mm] measured at 85% relative humidity as well as 35% relative humidity and $u_{(85)}$ as well as $u_{(35)}$ represent the

corresponding MC [%] of the specimens determined at 85% relative humidity and 35% relative humidity.

Furthermore, Eq. 3 was applied to calculate the MC in % of the specimens,

$$u = \frac{m_u - m_o}{m_o} \cdot 100 \quad (3)$$

where m_u is the mass [g] of the specimens at a given relative humidity and m_o is the oven-dry mass [g] of the specimens in completely dry condition.

Mathematical Model and Real FLM 3D Printed Specimens

The test specimens for the mathematical model and the FLM 3D printed ones were specially designed. There were several requirements for the specimen geometry to investigate the moisture-induced deformation behaviour of FLM 3D printed objects. Firstly, the specimens had to be of a sufficient size so that the deformation that occurs can be clearly measured. Secondly, it should be possible to measure the deformation behaviour at several points on a specimen in order to avoid partial material influences. Ideally, the specimens should have a symmetrical structure so that the independently occurring deformation behaviour on both sides can be directly compared with each other. With all these aspects in mind, both the shape as well as the geometry of the test specimen were determined.

Figure 2 shows the exact geometry of the samples, which had a length of 80 mm, a width of 35 mm, and a thickness of 10 mm. The three prongs had a length of 68 mm and a width of 2.4 mm respectively, whereby the two outer prongs were split into two 1.2 mm wide sections.

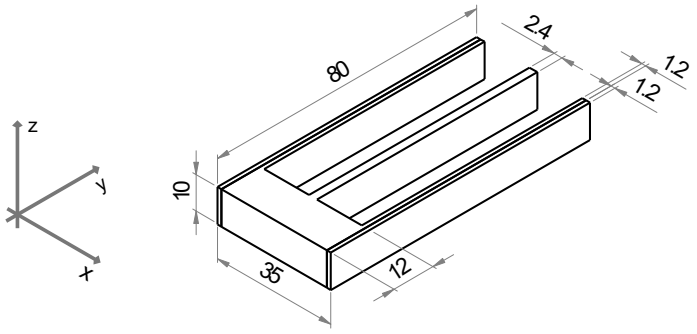

Fig. 2. Visualisation of the sample geometry for testing the moisture-induced shape changing behaviour as well as for evaluating the accuracy of the mathematical model (Dimensions in mm)

Only both outer prongs had alternating print directions, which deformed in a certain way depending on the prevailing climatic conditions. The middle section of the three-pronged test specimens always had the same structure, and no alternating print directions were applied. All deformations of the outer prongs were referenced to the non-deforming middle prong. Depending on the print directions applied, three different deformation types could be realised, as shown in Fig. 3.

A preliminary study with this specific NFC material showed that the extent of the swelling and shrinking behaviour was direction-dependent. It could be demonstrated in the study that the swelling and shrinking behaviour orthogonal to the print direction was considerably larger than parallel to the print direction. Therefore, it was assumed that a configuration where parallel to the print direction aligned areas are directly next to areas

aligned orthogonal to the print direction would have the maximum possible deformation, while all other combinations with regard to the print direction would lead to smaller deformations. For that reason, this specific configuration was utilized for the three-pronged specimens.

In total, three different deformation types were designed. These were 3D printed with FLM having alternating print directions. Type 1 resulted in an outward curvature of the outer prongs when these specimens got in contact with moisture. Type 2 showed no deformation at all when these specimens were exposed to moisture. Type 3 resulted in an inward curvature of the outer prongs when these specimens got in contact with moisture.

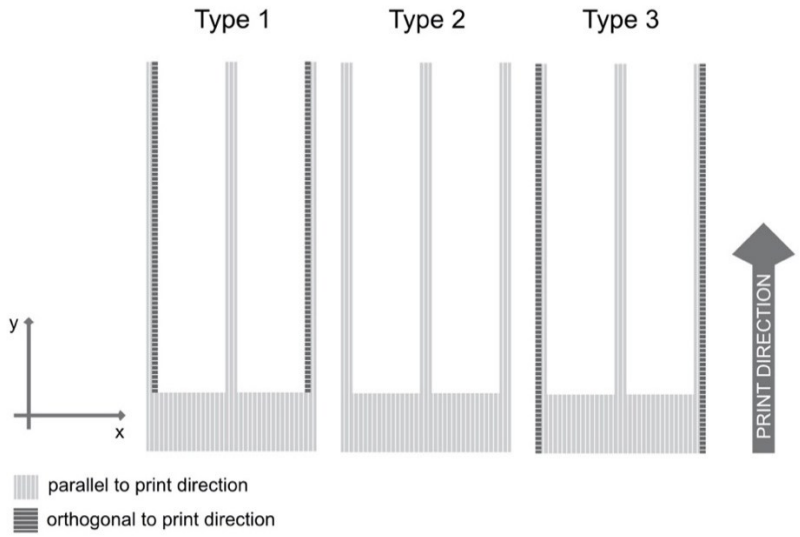

Fig. 3. Visualisation of the print directions applied for enabling a moisture-induced shape changing behaviour – 4D printing

The slicing software Cura (Version 3.2.1) was utilized for generating the gcode files. All of the process parameters applied for processing the specially fabricated wood/PLA filament can be seen in the publication by Kain *et al.* (2020). However, the wall thickness was set to 0 mm, meaning that there were no perimeters. In addition, the infill directions of the outer prongs of the samples were adjusted depending on which type of moisture-induced shape change should be achieved. A total of five identical test specimens were FLM 3D printed for each of the three types shown in Fig. 3.

In a first step, the FLM 3D-printed three-pronged specimens were accurately measured using the 3D scanner "Space Spider" from Artec 3D (Luxembourg, Luxemburg) and then conditioned in a climatic chamber with a temperature of 23 °C and 65% relative humidity. Afterwards, all test samples were exposed to a temperature of 23 °C and 85% relative humidity until the weight remained constant. The test specimens per deformation type were then precisely measured using the 3D scanner. This measurement procedure was repeated for a temperature of 23 °C and 50% relative humidity as well as for a temperature of 23 °C and 35% relative humidity. Finally, the specimens were gently dried in a kiln dryer at a temperature of 50°C until constant weight was reached. Thereafter, all test samples were accurately measured using the same 3D scanner. Subsequently, the variance in deformation between the undeformed state immediately after FLM 3D printing and the deformed state depending on the prevailing climatic condition was determined, resulting in the moisture-induced shape changing behaviour.

Mathematical Model

The simulation of the moisture-induced shape change was realised based on the mathematical model presented by Schnabel *et al.* (2017). This model is based on the linear difference method and was primarily developed to accurately predict the material deformation during wood drying. Due to material specific process parameters (*e.g.* print direction, print speed, *etc.*) while FLM 3D printing the test specimens, several modifications of the model had to be made.

The three-pronged test specimens were virtually segmented into 17 rectangular bar elements having different dimensions, one being illustrated in Fig. 4.

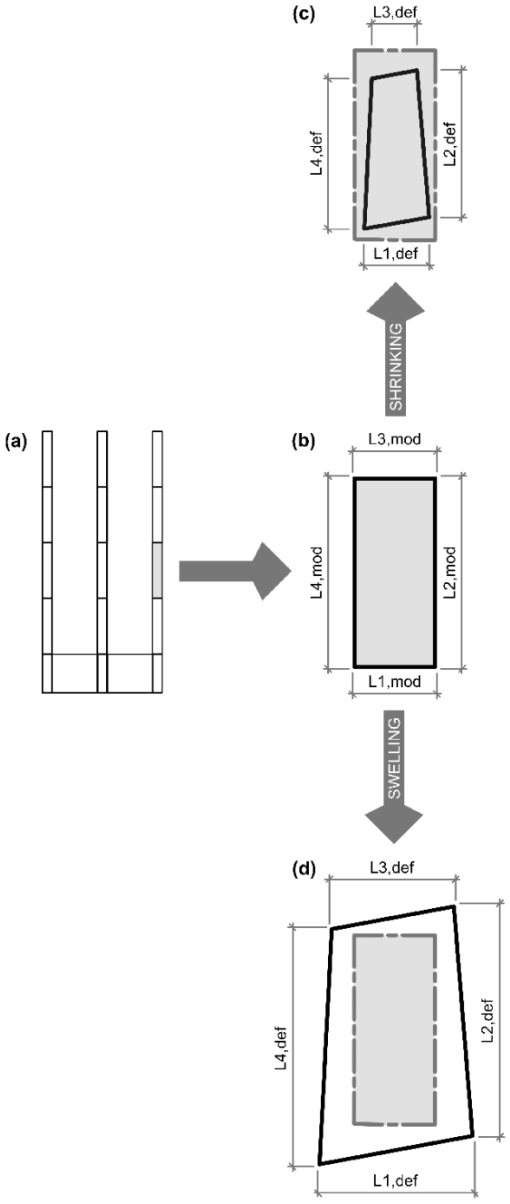

Fig. 4. Illustration (a) demonstrates the segmentation of the three-pronged test specimens (b) shows an undeformed segmented bar element while figure (c) and (d) illustrate a deformed one caused by shrinking as well as swelling

For estimating the deformations, the bar elements were calculated based on following criteria and parameters:

1) The MC values of the FLM 3D printed specimens are dependent on the ambient climate and were determined according to Eq. 3. The moisture change Δu [%] is a specific parameter which was included in the calculation according to Eq. 4. It was calculated in the following way,

$$\Delta u = u_{\text{def}} - u_{\text{print}} \quad (4)$$

where u_{def} is the MC level in % of the deformed specimens and u_{print} [%] represents the MC of the specimens immediately after FLM 3D printing. All moisture changes were related to the MC level immediately after FLM 3D printing, as the FLM 3D printer produced the initial shape.

2) The moisture-induced shape change was calculated based on the change in MC as well as the print directions applied. Therefore, each single bar element of the 17 within one specimen was identified according to its print directions (parallel $\beta_{\parallel}$ or orthogonal $\beta_{\perp}$). The differential swelling and shrinking behaviour was given by Eqs. 1 as well as 2 and was used to calculate the change in the bar element length $L_{\text{i,def}}$ [mm] according to Eq. 5, which was computed in the following way:

$$L_{i,\text{def}} = L_{i,\text{mod}} \cdot \beta_{\text{dir}} \cdot \Delta u \quad (5)$$

where $L_{\text{i,mod}}$ represents the original length [mm] of the bar element i after FLM 3D printing, β_{dir} [%/%] is the differential swelling and shrinking behaviour according to the print directions (parallel $\beta_{\parallel}$ or orthogonal $\beta_{\perp}$), and Δu [%] represents the moisture change.

The principle of the shape change calculation is exemplified in Fig. 4 for a drying process (the bar element shrinks) as well as for a wetting process (the bar element swells). It can be seen that the shape change for a bar element is assumed to be linear. After segmenting the FLM 3D printed geometry into 17 bar elements, the deformation was calculated for all of these bar elements. Based on the deformations of the single bar elements the overall shape change could be calculated and modelled.

3D Scanning of the Moisture-Induced Shape Deformations

The high-resolution handheld 3D scanner "Space Spider" from Artec 3D was utilized to capture the moisture-induced shape changes of the FLM 3D printed test specimens. This 3D scanner uses blue light technology for the scanning process and is very suitable for capturing small objects with fine details.

For each specimen, multiple scans were taken of the top and the bottom side while the specimen rotated on a work area, allowing for high-resolution 360° scans. The multiple scans per specimen were then merged using Artec's company-owned software Studio 13 Professional. In addition, this program was also utilized to evaluate the moisture-induced shape changing behaviour by superimposing the 3D scans of the undeformed and deformed specimens. In other words, the deformation of the outer prongs in comparison to the undeformed middle prong was determined as a function of the prevailing climate. Figure 5 shows the three different types of deformation for the FLM 3D printed three-pronged test specimens when in contact with a temperature of 23 °C and a relative humidity of 85%.

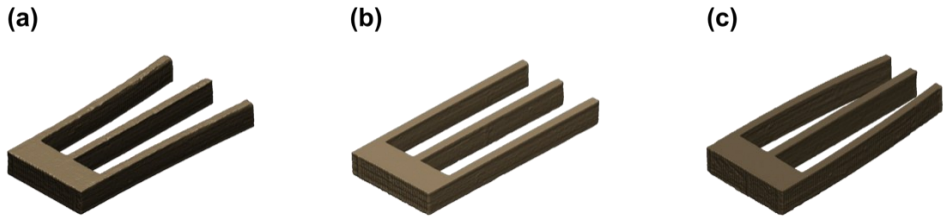

Fig. 5. 3D scan images of the deformed FLM 3D printed specimens once they came into contact with a temperature of 23 °C and a relative humidity of 85%. Three different types of deformation were investigated. Type 1, represented by (a), shows an outward curvature of the outer prongs when in contact with moisture. Type 2, represented by (b), shows no deformation at all. Type 3, represented by (c), shows an inward curvature of the outer prongs when in contact with moisture

RESULTS AND DISCUSSION

Moisture-Induced Swelling and Shrinking Parameters

Figure 6 illustrates the results of the differential swelling and shrinking behaviour of the test specimens shown in Fig. 1. It can be observed that there was a noticeable variation in terms of the print directions applied. An arithmetic mean of 0.10%/% was calculated for the differential swelling and shrinking behaviour parallel to the print direction ($\beta_{\parallel}$) – represented by the measuring sections No. 1, No. 2 and No. 3. For the differential swelling and shrinking behaviour orthogonal to the print direction ($\beta_{\perp}$) – represented by the measuring sections No. 4, No. 5 and No. 6 – an arithmetic mean of 0.31%/% was calculated. Basically, the differential swelling and shrinking behaviour $\beta_{\perp}$ was about three times higher than $\beta_{\parallel}$, which means that this specially made NFC had an anisotropic swelling and shrinking behaviour similar to certain wood species such as spruce or fir (Wagenführ 2007).

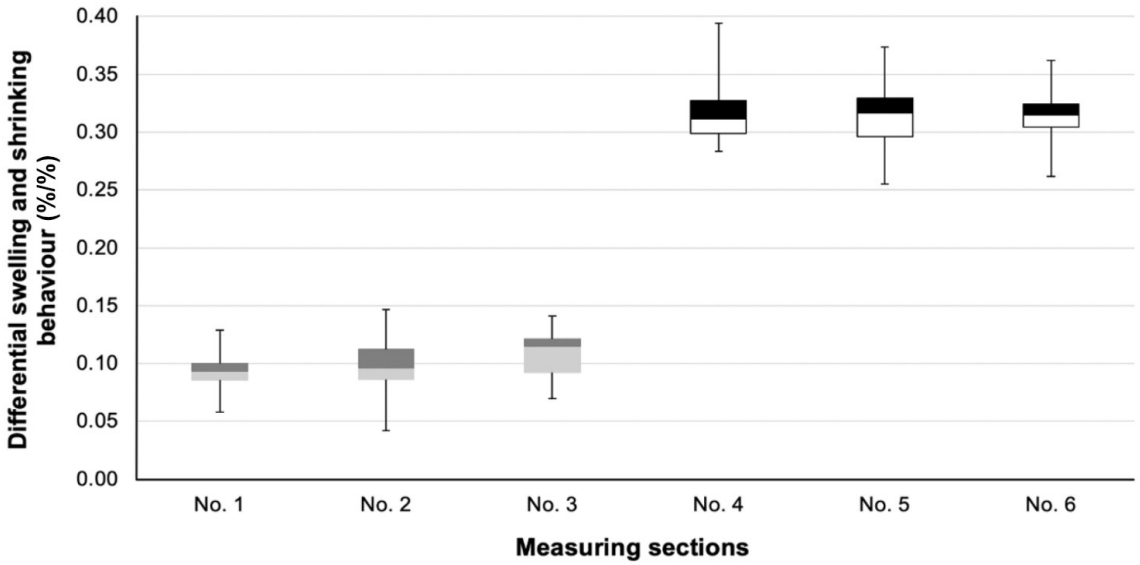

Fig. 6. The differential swelling and shrinking behaviour of the ten FLM 3D printed specimens (as illustrated in Fig. 1) is displayed. No. 1, No. 2, as well as No. 3 represent the measuring sections parallel to the print direction ($\beta_{\parallel}$), while No. 4, No. 5, and No. 6 represent the measuring sections orthogonal to the print direction ($\beta_{\perp}$).

Furthermore, the MC of the specimens – shown in Fig. 1 – was calculated as a function of the prevailing climatic conditions (temperature and relative humidity). When the test specimens were exposed to a temperature of 23 °C and 85% relative humidity, an arithmetic mean of 2.69% (u_{wet}) was calculated for the MC level. An arithmetic mean of 1.67% ($u_{standard}$) was determined for the MC level when the specimens were stored in a climatic chamber with a temperature of 23 °C and 50% relative humidity. When the test samples were in contact with a temperature of 23 °C and 35% relative humidity, an arithmetic mean of 1.32% (u_{dry}) was calculated for the MC level. For the test specimens immediately after FLM 3D printing, an arithmetic mean of 0.42% (u_{print}) was determined for the MC level.

Simulated Deformations *vs.* FLM 3D Printed Specimens

In Tables 2 and 3 the calculated parameters for the differential swelling and shrinking behaviour parallel as well as orthogonal to the print direction and the MC level as a function of the climatic conditions applied are illustrated.

Table 2. Average Differential Swelling and Shrinking Behaviour Parallel and Orthogonal to the Print Direction

$\beta_{\parallel}$	Diff. swelling and shrinking behaviour parallel to the print direction	0.10%/%
$\beta_{\perp}$	Diff. swelling and shrinking behaviour orthogonal to the print direction	0.31%/%

Table 3. Average MC Levels of the FLM 3D Printed Test Specimens – Shown in Fig. 1 – Depending on the Climatic Conditions Applied

u_{wet}	Temperature 23 °C and 85% relative humidity	2.69%
$u_{standard}$	Temperature 23 °C and 50% relative humidity	1.67%
u_{dry}	Temperature 23 °C and 35% relative humidity	1.32%
u_{print}	Immediately after FLM 3D printing	0.42%

Table 4 presents a comparison of the actually measured moisture-induced deformations of the FLM 3D printed three-pronged test specimens and the simulated deformations from the modified mathematical model (Schnabel *et al.* 2017) for all three types. At a temperature of 23 °C and 85% relative humidity, an averaged deformation of 20.7 mm (L_{left}) and 20.9 mm (L_{right}) could be determined for the FLM 3D printed representatives of type 1. The modified mathematical model (*Schnabel et al.* 2017) predicted a deformation of 20.8 mm respectively (L_{left} and L_{right}) for the same climatic condition, which means a deviation of -0.17% (L_{left}) and 0.72% (L_{right}) compared to the actually measured deformations. For representatives of type 2, no deformations (neither inward nor outward curvatures) could be observed when the specimens were exposed to the same climate condition. The prediction model also showed no deformations at all for the three-pronged specimens of type 2.

The FLM 3D printed representatives of type 3 obtained the following averaged characteristic values for the moisture-induced shape changing behaviour: L_{left} = 11.9 mm and L_{right} = 12.3 mm. The modified mathematical model (Schnabel *et al.* 2017) predicted a deformation of 11.6 mm respectively (L_{left} and L_{right}) for a temperature of 23 °C and 85% relative humidity, implying a deviation percentage of 2.65% (L_{left}) and 6.41% (L_{right}) compared to the actually measured deformations.

Table 4. Comparison of Actually Measured Deformations and the Simulated Ones Based on the Modified Mathematical Model (Schnabel *et al.* 2017) for a Temperature of 23 °C and 85% Relative Humidity

	Type 1	Type 2	Type 3
Actually measured deformations of the FLM 3D printed specimens *	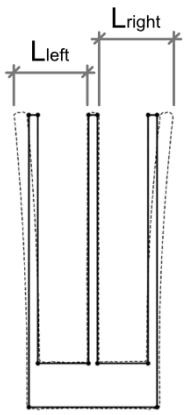	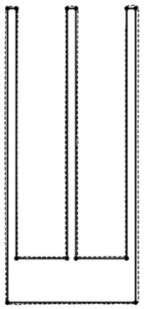	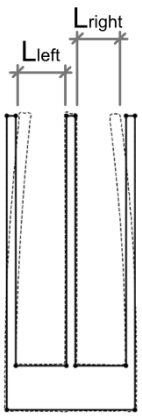
Simulated deformations	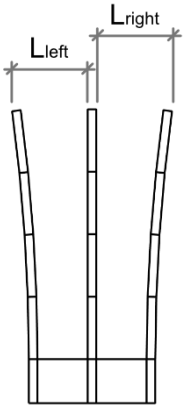	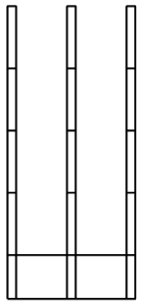	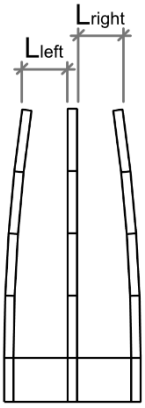

* The solid lines represent the undeformed specimens and the dotted lines stand for the deformed ones.

Table 5 illustrates for all types of deformation and all tested climatic conditions the overall comparison of the actually measured moisture-induced deformations of the FLM 3D printed three-pronged test specimens with the simulated ones gained from the modified mathematical model (Schnabel *et al.* 2017). It is striking, with a few exceptions (a maximal deviation rate of 6.41% when comparted to the actually measured deformations), that the prediction very accurately reflected the actually measured deformations of the FLM 3D printed three-prong specimens. This supports the precision of the modified mathematical model (Schnabel *et al.* 2017).

Slight deviations from the modified mathematical model (Schnabel *et al.* 2017) are also due to the fact that this is a two-dimensional approach to predict deformations of 4D printed objects and not a three-dimensional approach. Influences that would arise in a three-dimensional mathematical model over the layer height, *e.g.* shear ratios, can in no way be taken into account in such a two-dimensional model.

Table 5. Comparison of Actually Measured Deformations with the Simulated Ones Based on the Modified Mathematical Model (Schnabel *et al.* 2017) as a Function of the Different Climatic Conditions Applied and the Various Types of Deformation (*wet*, *standard* and *dry*)

Samples		Climate conditions											
		WET Temperature: 23 °C Relative humidity: 85%				**STANDARD** Temperature: 23 °C Relative humidity: 50%				**DRY** Temperature: 23 °C Relative humidity: 35%			
		Real deformations		Simul. defor.	Dev.	Real deformations		Simul. defor.	Dev.	Real deformations		Simul. defor.	Dev. rate
		$\bar{x}$	SD			$\bar{x}$	SD			$\bar{x}$	SD		
		(mm)	(mm)	(mm)	(%)	(mm)	(mm)	(mm)	(%)	(mm)	(mm)	(mm)	(%)
Type 1	L_{left}	20.74	0.27	20.77	**-0.17**	19.05	0.25	18.76	**1.53**	18.44	0.17	18.07	**2.03**
	L_{right}	20.92	0.14		**0.72**	19.34	0.24		**3.11**	18.62	0.15		**3.05**
Type 2	L_{left}	---	---	---	**---**	---	---	---	**---**	---	---	---	**---**
	L_{right}	---	---		**---**	---	---		**---**	---	---		**---**
Type 3	L_{left}	11.89	0.76	11.58	**2.65**	13.60	0.51	13.70	**-0.70**	14.29	0.52	14.43	**-0.99**
	L_{right}	12.32	0.46		**6.41**	14.15	0.36		**3.29**	14.70	0.42		**1.90**

Real deformations: Actually measured deformations of the FLM 3D printed specimens; Simul. defor.: Simulated deformations; Dev. rate: Deviation rate; $\bar{x}$: Arithmetic mean; SD: Standard deviation

Therefore, it can be assumed that a comprehensive three-dimensional mathematical model would accurately represent occurring deformations.

Furthermore, it can be seen that the average deviation between the left (L_{left}) and the right prongs (L_{right}) within one type of deformation was always below 0.56 mm. However, the majority of the average deviations lay in a range between 0.18 and 0.43 mm. These results show that the FLM 3D printed three-pronged test specimens exhibited a fairly uniform deformation behaviour. Nevertheless, there were deviations that were most likely due to the hygroscopic nature of the material used and the FLM 3D printing process itself. In the publication by Kain *et al.* (2020), SEM images of the test specimens showed randomly distributed imperfections – small bubbles – in the structure of the FLM 3D printed objects, resulting in a possible deviant behaviour of the material. The assumption was that moisture had accumulated in the material and during the printing process the moisture within the material changed to a gaseous state and thus formed these imperfections. Since the wood/PLA composite used and the process parameters applied were similar, it is reasonable to assume that the same imperfections occurred. The randomly distribution of these imperfections probably affected also the swelling and shrinkage behaviour of the manufactured three-pronged test specimens and ultimately led to the small deviations in terms of the moisture-induced deformation behaviour between the left (L_{left}) and the right prongs (L_{right}).

In addition, Figs. 7 and 8 show the moisture-induced deformation behaviour for type 1 as well as type 3 specimens depending on the prevailing climatic conditions (*wet, standard* and *dry*). *Wet* stands for deformations measured at a temperature of 23 °C and a relative humidity of 85%, *standard* represents deformations determined at a temperature of 23 °C as well as 50% relative humidity and *dry* stands for deformations measured at a temperature of 23 °C and a relative humidity of 35%. Furthermore, the determined deformations of the FLM 3D printed three-pronged test specimens were compared with the simulated ones, indicated by the dotted lines.

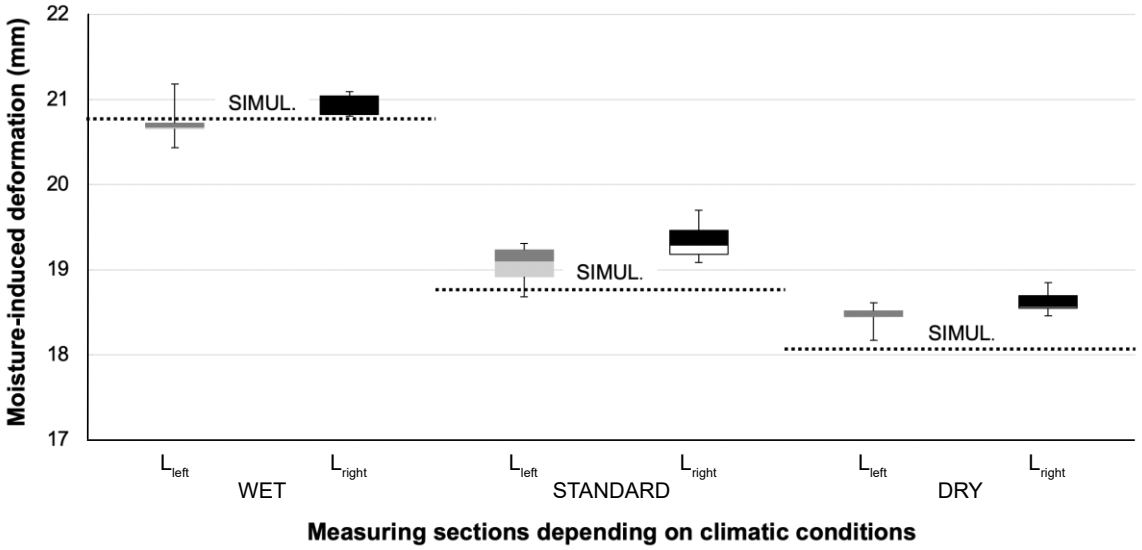

Fig. 7. Diagram of the moisture-induced deformations of type 1 specimens for different climatic conditions, where *wet* stands for a temperature of 23 °C and a relative humidity of 85%, *standard* represents a temperature of 23 °C and 50% relative humidity and *dry* stands for a temperature of 23 °C and a relative humidity of 35%. The dotted lines represent the simulated moisture-induced deformation values.

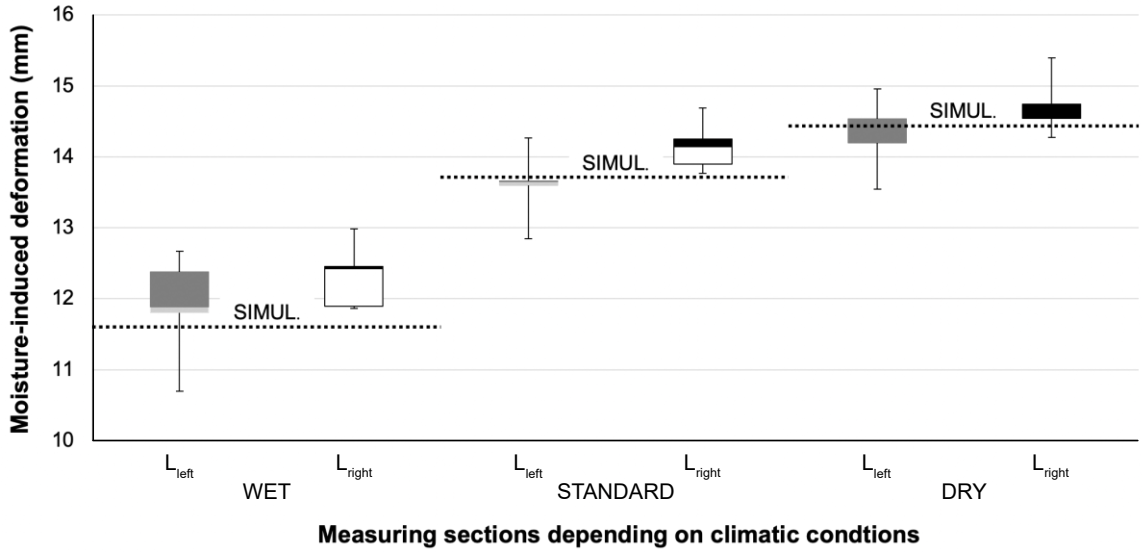

Fig. 8. Diagram of the moisture-induced deformations of type 3 specimens for different climatic conditions, where *wet* stands for a temperature of 23 °C and a relative humidity of 85%, *standard* represents a temperature of 23 °C and 50% relative humidity and *dry* stands for a temperature of 23 °C and a relative humidity of 35%. The dotted lines represent the simulated moisture-induced deformation values.

Figures 7 and 8 show that the predicted moisture-induced deformations based on the simulation were in many cases comparable to the deformations of the actual measured FLM 3D printed three-pronged specimens. Although there were discrepancies between the simulation and the actual measured deformations, the deviation percentage was always below 6.5%, which shows the potential of a two-dimensional simulation tool for accurate predictions of the moisture-induced deformation behaviour.

A simulation tool that is as accurate as possible could help to save valuable time, as the production of 4D printed test specimens and the tedious testing of the influence of varying print directions on the moisture-induced deformation behaviour would no longer be necessary. The moisture-induced deformations depending on the varying print directions as well as the prevailing climate can easily be taken from the simulation.

In the future, the following main research tasks will be investigated:

1. A noticeable improvement of the prediction accuracy of the modified mathematical model (Schnabel *et al.* 2017) by implementing time-dependent parameters.
2. An investigation of the effect of higher as well as lower wood fibre contents on the deformation behaviour of the FLM 3D printed objects.
3. Constructing and FLM 3D printing of several complex-shaped objects and attempting to predict the deformation behaviour using the modified mathematical model (Schnabel *et al.* 2017).
4. Microscopic analysis, including micro-CT scans, should also be performed to investigate the structural composition of the wood/PLA composites before and after FLM 3D printing. Specifically, the fibre as well as the particle distribution and the orientation of the filler material within the polymer matrix should be analysed.

CONCLUSIONS

1. The fabricated wood filament exhibited anisotropic swelling and shrinking behaviour, similar to that of certain wood species such as spruce or fir (Wagenführ 2007). In principle, the differential swelling and shrinking behaviour orthogonal to the print direction ($\beta_{\perp}$) was found to be higher than that parallel to the print direction ($\beta_{\parallel}$) by a factor of 3.
2. By using the specially produced wood filament (75 wt.% PLA and 25 wt.% wood fibres) and alternating the print directions during FLM 3D printing, it was in general possible to produce objects that changed their shape in a predictable way when they came into contact with moisture.
3. It could be demonstrated that the modified mathematical model (Schnabel *et al.* 2017) was capable of accurately predicting the deformation behaviour of the FLM 3D printed three-pronged samples. The established model for simulating the prong deflection by taking the MC as well as the differential swelling and shrinking behaviour into account showed promising results. For all three different climatic conditions (*wet*: 23 °C and 85% relative humidity, *standard*: 23 °C and 50% relative humidity, *dry*: 23 °C and 35% relative humidity) an accurate prediction could be made, with a deviation always below 6.5%. Nevertheless, there are still obstacles that need to be overcome, for example to improve the modelling method for industrial applications.
4. Table 5 as well as Figs. 7 and 8 show that the averaged deviation between the left (L_{left}) and the right (L_{right}) prongs within a deformation type was always very small, less than 0.56 mm, which means that the samples within a deformation type were fairly uniform in terms of deformation behaviour.
5. Furthermore, it was observed that submerging the test samples in a water bath at room temperature led to a slower response to shape change than exposing the specimens to a humid climate. Therefore, it can be claimed that water vapor is capable of penetrating the FLM 3D printed structures much better than liquid water.

ACKNOWLEDGEMENTS

Half of the investigations were implemented within the Salzburg Center for Smart Materials (SCSM as well as SCSM 2.0), while the other half of the experiments were implemented within the project Interreg Austria – Bavaria AB 97 TFP Hy-Mat. The SCSM is a cooperation between the University of Salzburg as well as the University of Applied Sciences Salzburg. Its research activities aim to develop and process new and innovative materials based on biogenic resources. In terms of the project Interreg Austria – Bavaria AB 97 TFP Hy-Mat, the aim was the establishment of hybrid materials, such as wood filaments for FLM 3D printing.

The authors gratefully acknowledge the financial support of the Salzburg Center for Smart Materials (P1727558-IWB01), which in turn is funded by the EFRE (European Funds for Regional Development) and AWS (Austrian Wirtschafts Service). The authors would also like to express their sincere gratitude for the financial support provided by the follow-up project of the Salzburg Centre for Smart Materials (SCSM 2.0), a research project of the Salzburg University of Applied Sciences and the University of Salzburg,

which is funded by the federal state of Salzburg. Additionally, the authors also gratefully acknowledge the financial support provided by the European Regional Development Fund and Interreg V-A Program Austria – Bavaria 2014–2020 through the Interreg Austria – Bavaria project AB 97 TFP Hy-Mat.

AUTHOR CONTRIBUTIONS

S. Kain: Writing – original draft, Writing – review & editing, Conceptualization, Methodology, Investigation, Software, Visualisation; **J. V. Ecker:** Writing – review & editing; **B. Dorfner:** Investigation; **A. Haider:** Writing – review & editing, Resources; **T. M. Young:** Writing – review & editing; **T. Schnabel:** Software, Writing – review & editing; **M. Musso:** Supervision, Writing – review & editing; **A. Petutschnigg:** Software, Resources, Funding acquisition

REFERENCES CITED

Addington, D. M., and Schodek, D. (2005). *Smart Materials and New Technologies: For the Architecture and Design Professions*, Routledge, Abingdon-on-Thames, UK.

Arslan, H., Nojoomi, A., Jeon, J., and Yum, K. (2019). "3D printing of anisotropic hydrogels with bioinspired motion," *Advanced Science* 6(2), article 1800703. https://doi.org/10.1002/advs.201800703

Ayrilmis, N. (2018). "Effect of layer thickness on surface properties of 3D printed materials produced from wood flour/PLA filament," *Polymer Testing* 71, 163-166. https://doi.org/10.1016/j.polymertesting.2018.09.009

Clifford, D., Zupan, R., Brigham, J., Beblow, R., Whittock, M., and Davis, N. (2017). "Application of the dynamic characteristics of shape-memory polymers to climate adaptive building facades," in: *Proceedings of 12th Conference of Advanced Building Skins*, Bern, Switzerland, pp. 171-178.

Correa, D., Papadopoulou, A., Guberan, C., Jhaveri, N., Reichert, S., Menges, A., and Tibbits, S. (2015). "3D-printed wood: Programming hygroscopic material transformations," *3D Printing and Additive Manufacturing* 2(3), 106-116. https://doi.org/10.1089/3dp.2015.0022

Correa, D., Poppinga, S., Mylo, M. D., Westermeier, A. S., Bruchmann, B., Menges, A., and Speck, T. (2020). "4D pine scale: biomimetic 4D printed autonomous scale and flap structures capable of multi-phase movement," *Philosophical Transactions of the Royal Society A: Mathematical, Physical and Engineering Sciences* 378(2167). https://doi.org/10.1098/rsta.2019.0445

Dányádi, L., Móczó, J., and Pukánszky, B. (2010). "Effect of various surface modifications of wood flour on the properties of PP/wood composites," *Composites Part A: Applied Science and Manufacturing* 41(2), 199-206. https://doi.org/10.1016/j.compositesa.2009.10.008

Dominkovics, Z., Dányádi, L., and Pukánszky, B. (2007). "Surface modification of wood flour and its effect on the properties of PP/wood composites," *Composites Part A: Applied Science and Manufacturing* 38(8), 1893-1901. https://doi.org/10.1016/j.compositesa.2007.04.001

Le Duigou, A., Castro, M., Bevan, R., and Martin, N. (2016). "3D printing of wood fibre biocomposites: From mechanical to actuation functionality," *Materials and Design* 96, 106-114. https://doi.org/10.1016/j.matdes.2016.02.018

Faruk, O., Bledzki, A. K., Fink, H. P., and Sain, M. (2012). "Biocomposites reinforced with natural fibers: 2000-2010," *Progress in Polymer Science* 37(11), 1552-1596. https://doi.org/10.1016/j.progpolymsci.2012.04.003

Gandhi, M. V., and Thompson B. D. (1992). *Smart Materials and Structures*, Chapman and Hall, London, UK.

Gladman, A. S., Matsumoto, E. A., Nuzzo, R. G., Mahadevan, L., and Lewis, J. A. (2016). "Biomimetic 4D printing," *Nature Materials* 15(4), 413-418. https://doi.org/10.1038/nmat4544

Hu, G. F., Damanpack, A. R., Bodaghi, M., and Liao, W. H. (2017). "Increasing dimension of structures by 4D printing shape memory polymers via fused deposition modeling," *Smart Materials and Structures* 26(12), article 125023. https://doi.org/10.1088/1361-665X/aa95ec

Huang, Y., Löschke, S., and Proust, G. (2021). "In the mix: The effect of wood composition on the 3D printability and mechanical performance of wood-plastic composites," *Composites Part C: Open Access* 5, article 100140. https://doi.org/10.1016/j.jcomc.2021.100140

Juaristi, M., Gómez-Acebo, T., and Monge-Barrio, A. (2018). "Qualitative analysis of promising materials and technologies for the design and evaluation of climate adaptive opaque façades," *Building and Environment* 144, 482-501. https://doi.org/10.1016/j.buildenv.2018.08.028

Kaboorani, A. (2017). "Characterizing water sorption and diffusion properties of wood/plastic composites as a function of formulation design," *Construction and Building Materials* 136, 164-172. https://doi.org/10.1016/j.conbuildmat.2016.12.120

Kain, S., Ecker, J. V., Haider, A., Musso, M., and Petutschnigg, A. (2020). "Effects of the infill pattern on mechanical properties of fused layer modeling (FLM) 3D printed wood/polylactic acid (PLA) composites," *European Journal of Wood and Wood Products* 78(1), 65-74. https://doi.org/10.1007/s00107-019-01473-0

Kariz, M., Sernek, M., and Kuzman, M. K. (2018). "Effect of humidity on 3D-printed specimens from wood-PLA filaments," *Wood Research* 63(5), 917-922.

Keener, T. J., Stuart, R. K., and Brown, T. K. (2004). "Maleated coupling agents for natural fibre composites," *Composites Part A: Applied Science and Manufacturing* 35(3), 357-362. https://doi.org/10.1016/j.compositesa.2003.09.014

Kim, J. K., and Pal, K. (2010). *Recent Advances in the Processing of Wood-Plastic Composites*, Springer-Verlag, Berlin Heidelberg, Berlin, Heidelberg, Germany.

Kirchmajer, D. M., Gorkin III, R., and Panhuis, M. I. H. (2015). "An overview of the suitability of hydrogel-forming polymers for extrusion-based 3D-printing," *Journal of Materials Chemistry B* 3(20), 4105-4117.

Lee, A. Y., An, J., and Chua, C. K. (2017a). "Two-way 4D printing: A review on the reversibility of 3D-printed shape memory materials," *Engineering* 3(5), 663-674. https://doi.org/10.1016/J.ENG.2017.05.014

Lee, J. Y., An, J., and Chua, C. K. (2017b). "Fundamentals and applications of 3D printing for novel materials," *Applied Materials Today* 7, 120-133. https://doi.org/10.1016/j.apmt.2017.02.004

van Manen, T., Janbaz, S., and Zadpoor, A. A. (2018). "Programming the shape-shifting of flat soft matter," *Materials Today* 21(2), 144-163. https://doi.org/10.1016/j.mattod.2017.08.026

Mohanty, A. K., Drzal, L. T.. and Misra, M. (2002). "Novel hybrid coupling agent as an adhesion promoter in natural fiber reinforced powder polypropylene composites," *Journal of Materials Science Letters* 21(23), 1885-1888. https://doi.org/10.1023/A:1021577632600

Pang, S. (2002). "Predicting anisotropic shringkage of softwood Part 1: Theories," *Wood Science and Technology* 36(1), 75-91. https://doi.org/10.1007/s00226-001-0122-4

Ratna, D., and Karger-Kocsis, J. (2008). "Recent advances in shape memory polymers and composites: a review," *Journal of Materials Science* 43(1), 254-269. https://doi.org/10.1007/s10853-007-2176-7

van Rees, W. M., Vouga, E., and Mahadevan, L. (2017). "Growth patterns for shape-shifting elastic bilayers," in: *Proceedings of the National Academy of Sciences of the United States of America* 114(44), Washington, USA, pp. 11597-11602. https://doi.org/10.1073/pnas.1709025114

Reichert, S., Menges, A., and Correa, D. (2015). "Meteorosensitive architecture: Biomimetic building skins based on materially embedded and hygroscopically enabled responsiveness," *Computer-Aided Design* 60, 50-69. https://doi.org/10.1016/j.cad.2014.02.010

Schnabel, T., Hermann H., and Petutschnigg, A. (2017). "Modelling and simulation of deformation behaviour during drying using a concept of linear difference method," *Wood Science and Technology* 51(3), 463-473. https://doi.org/10.1007/s00226-017-0897-6

Studart, A. R. (2015). "Biologically inspired dynamic material systems," *Angewandte Chemie - International Edition* 54(11), 3400-3416. https://doi.org/10.1002/anie.201410139

Thompson, B. S., Gandhi, M. V., and Kasiviswanathan, S. (1992). "An introduction to smart materials and structures," *Materials and Design* 13(1), 3-9. https://doi.org/10.1016/0261-3069(92)90045-J

Vailati, C., Bachtiar, E., Hass, P., Burgert, I., and Rüggeberg, M. (2018). "An autonomous shading system based on coupled wood bilayer elements," *Energy and Buildings* 158, 1013-1022. https://doi.org/10.1016/j.enbuild.2017.10.042

Vazquez, E., Gursoy, B., and Duarte, J. (2019). "Designing for shape change: a case study on 3D printing composite materials for responsive architecture," in: *Proceedings of Intelligent and Informed - 24th International Conference on Computer-Aided Architectural Design Research* 2, Wellington, Neuseeland, pp. 391-400.

Wagenführ, R. (2007). *Holzatlas (Atlas of Wood)*, 6th Edition, Neu bearbeitete und erweiterte Auflage, Fachbuchverlag Leipzig im Hanser-Verlag, München, Germany (in German).

Wang, Q., Sun, J., Yao, Q., Ji, C., Liu, J., and Zhu, Q. (2018). "3D printing with cellulose materials," *Cellulose* 25(8), 4275-4301. https://doi.org/10.1007/s10570-018-1888-y

Wei, Z. G., Sandström, R., and Miyazaki, S. (1998). "Shape-memory materials and hybrid composites for smart systems - Part I Shape-memory materials," *Journal of Materials Science* 33(15), 3743-3762. https://doi.org/10.1023/A:1004692329247

Wimmer, R., Steyrer, B., Woess, J., Koddenberg, T., and Mundigler, N. (2015). "3D printing and wood," *Pro Ligno* 11(4), 144-149.

Yu, K., Ritchie, A., Mao, Y., Dunn, M. L., and Qi, H. J. (2015). "Controlled sequential shape changing components by 3D printing of shape memory polymer multi-materials," *Procedia Iutam* 12, 193-203. https://doi.org/10.1016/j.piutam.2014.12.021

Zafar, M. Q., and Zhao, H. (2020). "4D printing: Future insight in additive manufacturing," *Metals and Materials International* 26(5), 564-585. https://doi.org/10.1007/s12540-019-00441-w

Zuluaga, D. C., and Menges, A. (2015). "3D printed hygroscopic programmable material systems," *MRS Online Proceedings Library (OPL)* 1800. https://doi.org/10.1557/opl.2015.644

Article submitted: October 14, 2021; Peer review completed: November 14, 2021; Revised version received: November 22, 2021; Accepted: December 10, 2025; Published: February 16, 2026.
DOI: 10.15376/biores.21.2.3137-3157